Applied Catalysis A: General 524 (2016) 85–93

Contents lists available at ScienceDirect

Applied Catalysis A: General

journal homepage: www.elsevier.com/locate/apcata

Investigating the multifunctional nature of bimetallic FeMoP catalysts using dehydration and hydrogenolysis reactions

Dallas J. Rensel, Jongsik Kim, Yolanda Bonita, Jason C. Hicks*

University of Notre Dame, Department of Chemical and Biomolecular Engineering, 182 Fitzpatrick Hall, Notre Dame, IN 46556, United States

ARTICLE INFO

Article history:
Received 26 February 2016
Received in revised form 18 May 2016
Accepted 7 June 2016
Available online 9 June 2016

Keywords:
Hydrodeoxygenation
Dehydration
Bimetallic
Phosphides
Catalyst
Biofuels

ABSTRACT

Herein, we investigate the effects of altering the multifunctional nature of a series of FeMoP catalysts for biomass deoxygenation reactions. Unsupported FeMoP catalysts were synthesized at reduction temperatures between 650 °C and 850 °C. The reduction temperature used during the synthesis of FeMoP altered the surface properties of these materials (i.e., acidity and CO-titrated metal sites) while leaving the bulk crystal structure of FeMoP unaffected. This alteration in the surface properties significantly affected the catalytic performance of FeMoP materials in the deoxygenation reactions. The catalytic performance of the FeMoP catalysts was first investigated using the acid catalyzed, non-aqueous, dehydration of cyclohexanol. Aside from showing high selectivities to cyclohexene (>99%) for all catalysts, the experiments demonstrated that FeMoP-650 showed the highest initial rate due to the largest number of surface acid sites among these catalysts. In addition, these FeMoP catalysts were examined using the hydrodeoxygenation (HDO) of phenol. While all FeMoP catalysts were highly selective to benzene (~90%) at conversions less than 15%, studies at higher conversions of phenol provided evidence that catalysts with a higher amount of acid sites maintained enhanced selectivity to benzene. Furthermore, the stability of FeMoP catalysts for phenol HDO was tested with a 48 h time-on-stream (TOS) study. FeMoP exhibited excellent stability, as evidenced by the retention of the initial reaction rate, selectivity to benzene, and oxidation state of surface species throughout the TOS run.

1. Introduction

Lignocellulosic biomass is an abundant and renewable resource from which to derive value-added chemicals and hydrocarbons [1–5]. In particular, the lignin portion of biomass, primarily consisting of phenolic ethers, is the largest source of aromatic compounds in nature [6]. It has been demonstrated that phenolic ethers can be catalytically transformed into a wide range of aromatic feedstocks primarily via deoxygenation reactions (e.g. hydrodeoxygenation (HDO)) [6]. Many transition metal catalysts, such as sulfides [7,8], noble metals [9–12], and carbides [13,14], have been studied for lignin and lignin model compound deoxygenation reactions at elevated temperatures (e.g., >200 °C) [15]. While these catalysts have shown high activities for these reactions, they suffered from either low selectivities to aromatic products (i.e., noble metals [16–18]) and/or low stability during the reaction (i.e., sulfides [19,20], oxides [21], and carbides [22]) due in part to (1) preferential hydrogenation of $C_{AROMATIC}$-H over $C_{AROMATIC}$-O and (2) chemical susceptibility to coking and oxidation resulting from the oxygenated products.

To obtain a good balance of activity, selectivity, and stability for catalytic deoxygenation of lignin and its derivatives, the catalysts should provide the following surface properties: (1) acid sites to aid in the removal of —OH functional groups innate to lignin derivatives [23,24], (2) metal sites to adsorb lignin derivatives and catalyze HDO [13,25], and (3) coking and oxidation resistance under the reaction conditions employed [19–21]. Mono-metallic transition metal phosphides represent an interesting and amenable class of catalysts that can provide a unique combination of surface acidic and metallic species active for the deoxygenation of lignin [25–27]. Monometallic phosphide catalysts (e.g., Ni_2P, Co_2P, MoP, and FeP [28]), however, have been reported with low yields or low selectivities toward aromatic products in these reactions and exhibited low stability due potentially to surface oxidation during the reactions [28–30]. A highly promising method to modify the surface properties of phosphide catalysis is to incorporate a second metal into the mono-metallic structure to form a bimetallic structure. Bimetallic phosphides have been reported as catalysts with increased selec-

* Corresponding author.
E-mail address: jhicks3@nd.edu (J.C. Hicks).

http://dx.doi.org/10.1016/j.apcata.2016.06.011
0926-860X/

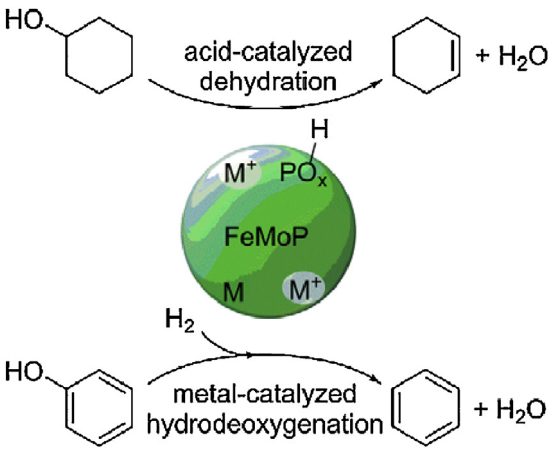

Fig. 1. Schematic representation of the multifunctional properties of FeMoP catalytically deoxygenating two lignin model compounds.

tivity to aromatic products compared to mono-metallic phosphides in a variety of deoxygenation reactions [29,31–33]. In addition to retaining surface acidity and surface metal sites, the incorporation of the second transition metal provides another method to enhance the chemical, electronic, and surface properties of the phosphide catalysts [25]. Moreover, the catalytic properties of bimetallic phosphides can be tuned for improved performance by altering phosphide synthesis conditions, expanding the application of these materials to a variety of reactions [27,33]. However, there has not been a systematic study performed to elucidate the impact of synthetic conditions on surface properties and HDO catalytic performance.

In spite of the aforementioned potential of these materials, there have been few reports detailing the effects of bimetallic phosphide synthesis conditions on their catalytic surface properties [33]. In a previous study, we employed bimetallic FeMoP as a catalyst to cleave $C_{AROMATIC}$-O bonds of anisole, phenol, and phenethoxybenzene, which resulted in the production of deoxygenated aromatic compounds (e.g. benzene, toluene, ethylbenzene) with high selectivities (~90%) over the production of saturated compounds (e.g. cyclohexane) [27]. The FeMoP catalyst also showed good stability for the deoxygenation of phenol, as it was able to catalyze this transformation for five consecutive reaction cycles with almost no loss in selectivity [27].

Herein, we varied the FeMoP reduction temperature to investigate the effects of synthesis conditions on catalytic surface properties (i.e., the number of surface acid and metal sites) and how these surface properties subsequently affected catalytic performance in deoxygenation reactions. Specifically, the multifunctional surface properties of the FeMoP catalysts were investigated using the catalytic deoxygenation of two lignin model compounds, cyclohexanol (with $C_{ALIPHATIC}$-O) and phenol (with $C_{AROMATIC}$-O)], as probe reactions. The effect of acid sites present on the FeMoP surface was probed via the non-aqueous, dehydration of cyclohexanol, whereas the effect of metal sites (i.e. CO-titrated metal sites) on the FeMoP surface was studied via the HDO of phenol (Fig. 1). In addition, mechanistic studies were performed in order to understand how the combination of acid sites and metal sites affected the product selectivity for the HDO of phenol. In addition to detailed catalytic studies using these two reactions, the stability of the FeMoP catalysts was also evaluated via a 48h time-on-stream (TOS) experiment for the HDO of phenol. From these detailed experiments, it is evident that FeMoP catalysts can have a significant impact on deoxygenation reactions pertinent to biomass utilization and biofuels/bio-chemicals production.

2. Experimental methods

2.1. Chemicals

All materials were used as-received with no further purification: citric acid (Alfa Aesar, 99%), $FeNO_3{\cdot}9H_2O$ (Alfa Aesar, 99%), $(NH_4)_6Mo_7O_{24}{\bullet}4H_2O$ (Alfa Aesar, 99%), $(NH_4)_2HPO_4$ (Amresco, 98%), phenol (Sigma-Aldrich, 99%), cyclohexanol (Alfa Aesar, 99%), benzene (Alfa Aesar, 99%), cyclohexene (Alfa Aesar, 99%), cyclohexane (Acros Organics, 99%) decane (Alfa Aesar, 99%), and Davisil® silica gel (Sigma Aldrich, Grade 635, 60–100 mesh). All gas cylinders (purity of ≥99.995%) were purchased from Airgas: Ar, He, N_2, H_2, 1% O_2/He, 2% NH_3/He, and 30% CO/He.

2.2. Synthesis of FeMoP catalysts

FeMoP catalysts were synthesized according to a slightly modified procedure we previously reported [27]. $FeNO_3{\cdot}9H_2O$, $(NH_4)_6Mo_7O_{24}{\cdot}4H_2O$, and $(NH_4)_2HPO_4$ were added sequentially to an aqueous citric acid solution (0.4 M in deionized water) while achieving a molar ratio of Fe:Mo:P of 1:1:1. The solution was partially dried using a rotary evaporator to form a viscous liquid prior to being transferred to a drying dish. The viscous solution was further dried and calcined under an air atmosphere with a ramp rate of 1.5 °C min^{-1} to 200 °C and held at 200 °C for an hour. Subsequently, resulting intermediate was ground into a powder and then subjected to the calcination under the air atmosphere at 550 °C with a ramp rate of 1 °C min^{-1} and held at 550 °C for six hours. The resulting material was a mixture of $FePO_4$ and MoO_3. Afterwards, the resulting powder was reduced using a Lindberg Blue M programmable tube furnace under the following condition: drying at 100 °C for an hour under an Ar atmosphere with the flow rate of 60 mL min^{-1} followed by two-step reduction under a H_2 atmosphere with the flow rate of 160 mL min^{-1} (1st step: holding at 260 °C for an hour with the ramp rate of 5 °C min^{-1} (between 25 °C to 260 °C); 2nd step: holding at target temperatures (i.e., 650, 750, 800, and 850 °C) for two hours with the ramp rate of 5 °C min^{-1} (between 260 °C to target temperature)). After the reduction, the resulting FeMoP catalysts were cooled to room temperature under the H_2 atmosphere, passivated using a 1% O_2/He with the flow rate of 60 mL min^{-1} for an hour, and then transferred to a glovebox purged with a N_2 atmosphere (>99%). The resulting FeMoP catalysts were denoted as FeMoP-XXX, where XXX indicates the target reduction temperature employed under the 2nd reduction step.

2.3. Characterization

X-ray diffraction (XRD) patterns were collected using a Bruker DaVinci Advanced D8 X-ray diffractometer equipped with a Cu Kα radiation source (λ = 1.5418 Å) under a 2θ range of 20–60°, a scan speed of 3.5 s./step, and a size step of 0.02°/step. Crystallite size was evaluated using the Scherrer equation shown in Eq. (1), where K is the shape factor (0.9, based on prior work on phosphides [34]), λ is the wavelength of the Cu Kα source, β is the full width half max (FWHM) value of the peak, and θ is the Bragg angle.

$$crystallite\ size = \frac{K\lambda}{\beta cos\theta} \quad (1)$$

In situ transmission electron microscopy (TEM) images were acquired on a FEI Titan 80–300 microscope at 300 keV, equipped with *in situ* sample holder along with heating chip (DENS Solutions Corporation). The TEM samples were prepared by sonicating the catalyst in *iso*-propyl alcohol for 5 min, placing one drop of the suspension on the *in situ* sample holder, and then drying under vacuum (10^{-2} torr) at room temperature for 2 h prior to analysis. NH_3 temperature programmed desorption (NH_3-TPD) experiments

were conducted on a Micromeritics Chemisorb 2750 equipped with a thermal conductivity detector (TCD) and TPx temperature controller. The catalyst was re-reduced under a H_2 atmosphere by ramping at a rate of 10 °C min^{-1} to 400 °C for an hour. Chemisorption of NH_3 was performed at 100 °C for 3 h. Subsequently, NH_3 desorption was performed in flowing He by ramping at 10 °C min^{-1} to 230 °C, holding for 42 min, then ramping at 10 °C min^{-1} to 400 °C, and holding for 42 min. The desorbed area was quantified based on NH_3 calibrations determined using the 2% NH_3/He. CO chemisorption experiments were conducted on the Micromeritics Chemisorb 2750 instrument following the same pre-treatment steps as the NH_3-TPD experiments. Pulse chemisorption of CO was performed at 35 °C using 0.1 mL injections of a 30% CO/He. The CO uptake on each material was obtained by summing the area of each peak and subsequently quantified based on CO calibrations determined using 30% CO/He. Brunauer-Emmett-Teller surface area (S_{BET}) of the catalyst was analyzed using a Quantachrome Nova 2200e. A PHI VersaProbe II X-ray Photoelectron Spectrometer was used to obtain X-ray photoelectron (XP) spectra of the catalysts to analyze the surface species. The Fe $2p_{3/2}$, Mo $3d_{5/2}$, and P $2p_{3/2}$ peaks were used to compare binding energies based on a C 1s reference peak located at 284.5 eV.

2.4. Dehydration of cyclohexanol and HDO of phenol

All reactions were performed in a custom-built continuous flow reactor. For the kinetic studies, the reaction was operated in the forward reaction-dominant regime with the conversion of 15% or lower. In a typical experiment, 30 mg of the catalyst particles were diluted using 100 mg of Davisil® grade 635 and subsequently packed in a 316 stainless steel reactor equipped with a stainless mesh steel screen (10 μm, McMaster-Carr) and quartz wool (VWR Scientific) to immobilize the catalysts particles in the reactor. The reactor was operated in an up-flow configuration. Flow rates of reactant solutions (0.13 M of cyclohexanol dissolved in decane; 0.13 M of phenol dissolved in decane) were controlled using a high pressure liquid chromatography (HPLC) pump (Hitachi L-6000), whereas flow rates of gases (100 mL min^{-1} of N_2 for cyclohexanol; 100 mL min^{-1} of H_2 for phenol) were regulated using a mass flow controller (Aalborg GFC17). Reaction temperature was set using PID controllers and maintained at 180–220 °C (for cyclohexanol) and 350–400 °C (for phenol) using a heat tape (Omega Engineering) equipped on the reactor. HDO reactions were operated in an excess hydrogen flow with the feed molar ratio of H_2 to phenol as ~34. Catalytic results (i.e., conversion and selectivity) were quantified using an Agilent 7890A gas chromatograph (GC) directly coupled with an Agilent 5975C mass spectrometer (MS) based on external calibration curves of both reactants and products. Throughout all reaction runs, the carbon balance was 96% or greater. Conversion and selectivity were calculated based on Eqs. (2) and (3).

$$conversion = \frac{moles\ of\ reactant\ converted}{moles\ of\ reactant\ fed} \times 100 \quad (2)$$

$$selectivity = \frac{moles\ of\ specific\ product}{moles\ of\ all\ products} \times 100 \quad (3)$$

All reported reaction rates are initial rates calculated by using the rate expression discussed in the text and extrapolating to the initial solution concentration. The fitted rate law was validated based on the reactions run at 400 °C with varying concentrations of phenol and varying concentrations of H_2 using the FeMoP-650 catalyst.

3. Results and discussion

3.1. FeMoP catalysts syntheses and characterizations

The FeMoP catalysts were synthesized following a procedure we previously reported [27] except with varying reduction temperatures ranging from 400 °C to 850 °C (Fig. S1). This led to a series of FeMoP catalysts denoted as FeMoP-XXX (where XXX indicates the reduction temperature). The bulk crystal structures of the resulting FeMoP catalysts were investigated using X-ray diffraction (XRD). The purpose of this XRD analysis was to determine the range of reduction temperatures suitable for the production of the crystalline FeMoP structure. Aside from showing a peak assigned to a FeMoP diffraction (Fig. S2), the catalysts synthesized at 600 °C or below exhibited multiple diffractions attributed to bulk phases of Mo, MoO_2, MoO_3, $FePO_4$, and Fe_2PO_7, and thus were not studied as part of this work. In contrast, as shown in Fig. S3, the catalysts synthesized at 650 °C or greater showed only diffractions assigned to the crystalline FeMoP bulk phase, and thus were utilized in this study. Notably, the increase in reduction temperatures used during the synthesis of FeMoP catalysts resulted in the continuous growth of FeMoP crystallites, as evidenced by the increase in average crystallites size from 22 nm (650 °C) to 44 nm (850 °C) estimated using the Scherrer equation (Table 1). This crystallite growth was also consistent to transmission electron microscopy (TEM) images of FeMoP-550 heated *in situ* from 650 °C to 850 °C (Fig. S4). In this experiment, a single region containing the catalyst was imaged at different temperatures to show the change in morphology. These images revealed a significant morphological change at 800 °C, likely resulting from the aggregation of FeMoP crystallites. In agreement with the trend observed in both XRD and *in situ* TEM experiments, the increase in reduction temperatures also led to the decrease in BET surface areas (S_{BET}) of the resulting FeMoP catalysts as determined by N_2 physisorption experiments (Table 1).

The surface properties were investigated using x-ray photoelectron spectroscopy (XPS). XPS analysis provided evidence the surface of the FeMoP catalysts was composed of Fe, Mo, and P species that were close to their zero valence states or at a higher oxidation state (Fig. S5). The oxidation state of the species close to their zero valence state was not clearly assigned due to interatomic effects in phosphide materials that induced a Madelung potential (electrostatic interaction), as reported for several MP and M_2P materials (M = metal) [35,36]. These XP spectra also showed the presence of oxidized species such as Fe^{3+}, Mo^{6+}, and P^{5+} located at binding energies of 711.1 eV, 232.1 eV, and 133.5 eV, respectively [27,37,38]. The oxidized surface species were likely formed by either oxidation of the catalyst surface during passivation under 1% O_2 in He during synthesis or by the incomplete reduction to the FeMoP structure, both of which could provide Lewis and Brønsted surface acid sites ($M^{\delta+}$ as Lewis acid sites and M-OH and/or P-OH as Brønsted acid sites) on the catalysts. Additionally, several prior studies that synthesized monometallic phosphide catalysts reported the evolution of phosphide gas during reduction of the precursors [26,34,39]. To test the potential loss of P on the FeMoP catalysts, XPS was used to determine the ratio of metal atoms to P atoms. The surface composition of P on FeMoP reduced at 650, 750, 800, and 850 °C was 34, 32, 32, and 31 at.%, respectively. While it is possible that some P is removed at higher reduction temperatures, the surface concentration of P was fairly unaffected.

NH_3-temperature programmed desorption (TPD) was used to quantify the surface acid concentration (ρ_{ACID}, μmol m^{-2}, in Table 1) present on the FeMoP catalysts (Fig. S6) [29]. Prior reports investigating NiMoP, MoP, and Ni_2P have shown that two types of acid sites, Brønsted and Lewis, were present on the surface of phosphide materials [29,30,40]. One report suggested that NH_3 desorbed from these two acid sites at different temperatures,

Table 1
Physical properties of the FeMoP catalysts.

catalyst	average crystallite size[a,b] (nm)	S_{BET}[c] ($m^2\,g^{-1}$)	ρ_{ACID}[d] ($\mu mol\,m^{-2}$)	N_{CO}[e] ($\mu mol\,g^{-1}$)
FeMoP-650	22.0	6.8	3.9 ± 0.4	28.5 ± 2
FeMoP-750	26.4	2.7	3.2 ± 0.3	9.6 ± 0.7
FeMoP-800	39.2	1.8	2.2 ± 0.2	5.3 ± 0.4
FeMoP-850	44.2	1.5	1.0 ± 0.1	2.0 ± 0.2

[a] Via Scherrer equation.
[b] Average of values evaluated at (011), (200), and (211).
[c] Via N_2 physisorption.
[d] Areal acid concentration (ρ_{ACID}) via NH_3-TPD and S_{BET}.
[e] Via CO-pulsed chemisorption.

~210 °C for Brønsted acids and ~320 °C for Lewis acid sites [29]. The NH_3 TPD plots in Fig. S6 shows two separate peaks, one at low temperature (~210 °C) and at high temperature (~310 °C), which suggested that two different types of acid sites were present on the FeMoP materials. As shown in Table 1, the increase in reduction temperatures resulted in a decrease in ρ_{ACID}, which suggested that thermochemical reduction under a H_2 atmosphere eliminated surface acid sites on FeMoP catalysts at elevated temperatures. In addition, the loss of surface area from sintering observed in *in situ* TEM images could also lead to the decrease in ρ_{ACID}. The reduction in Brønsted acid sites was likely caused by H_2 that thermochemically cleaved the —OH groups on the surface of MP or M_1M_2P, liberating H_2O [41–43]. This was suggested based on the phase transition of metal oxide and phosphate materials, which showed the gradual elimination of surface Brønsted acid sites at reduction temperatures of 500 °C or greater [41–43]. The Lewis acid sites also decreased with an increase in reduction temperature. One possible reason for this decrease could be the heterolytic cleavage of H_2 to form $M^{\delta+}$-$H^{\delta-}$ surface species at higher reduction temperatures [44,45]. Other reports on supported metal phosphide catalysts (e.g., Ni_2P [40]) have clearly shown Brønsted and Lewis acid sites from Fourier Transform Infrared spectroscopy (FT-IR) analysis. Attempts to collect spectroscopic data of these acid sites on the unsupported FeMoP catalysts were unsuccessful because these samples were dark in color and had a poor spectroscopic reflectivity, which in turn showed only weak peak intensities in the FT-IR spectra. In addition to the investigation of ρ_{ACID} innate to the FeMoP catalysts, the quantity of CO-titrated surface metal sites (i.e. Lewis acid metal sites and metallic sites [46,47], N_{CO}) in the FeMoP catalysts were also determined via CO pulsed chemisorption experiments. Similar as the trend of ρ_{ACID}, the increase in reduction temperatures also reduced the quantity of N_{CO} (Table 1). The loss of CO-titrated surface sites in the FeMoP catalysts at elevated reduction temperatures was likely due to the loss in the surface area from the growth of FeMoP crystallites (Fig. S4).

3.2. Deoxygenation on the FeMoP catalysts

3.2.1. Dehydration of cyclohexanol

The effects of altering surface properties of the FeMoP on catalytic performance were then investigated using two lignin model compounds. Previously, surface acid sites (i.e. Brønsted and Lewis acid sites) in various catalysts have been shown to catalyze the dehydration of aliphatic alcohols with high selectivities to aliphatic alkenes [48,49]. Therefore, to determine if the acid sites on the FeMoP catalysts were accessible and catalytically active, the dehydration of cyclohexanol (a $C_{ALIPHATIC}$-OH compound, denoted as COH), a model compound that can be generated from the hydrogenation of lignin derivatives, was studied as a probe reaction [16,50]. The catalytic performances of the FeMoP catalysts for this reaction were evaluated using a flow reactor under a N_2 atmosphere (5.2 MPa) at 220 °C. All reaction runs were operated in the reaction-limited regime ($X_{CYCLOHEXANOL} \leq 15\%$) and utilized an identical amount of catalyst for each reaction (30 mg).

A 1st-order reaction assumption was used for the calculation of reaction rate based on previous reports with solid acid catalysts [16,51]. The initial rate of cyclohexanol consumption for each catalyst was calculated from the rate and concentration measured during reaction. The measured rate was used to determine the rate constant, which was then multiplied by the initial concentration of cyclohexanol to obtain the initial reaction rate. It should be noted that neither mass transport limitations nor reaction heat effects played significant roles during the kinetic evaluation. This was evidenced by three control reaction runs with FeMoP-650 at 220 °C (Fig. S7) which showed consistent values of $-r_{0,COH/MASS}$ under the employed reaction conditions (particle size = 60–100 mesh, flow rate = 1.0 mL min^{-1} solution, diluent ratio = 4 parts silica gel to 1 part catalyst), regardless of varying the size of the catalytic particles, flow rate of cyclohexanol, and amount of the diluent. The FeMoP-800 catalyst was excluded in this study due to its similar surface properties (e.g., ρ_{ACID} and S_{BET} in Table 1) to those of FeMoP-850. As expected, these reactions evolved cyclohexene with high selectivities (>99%) at all temperatures with all catalysts (FeMoP-650, FeMoP-750, and FeMoP-850). Values of $-r_{0,COH/MASS}$ for the FeMoP catalysts showed that the $-r_{0,COH/MASS}$ values decreased with an increase in the reduction temperatures used to synthesize the FeMoP catalysts. Furthermore, as stated above, an increase in reduction temperature also led to lower values of ρ_{ACID} (Fig. 2a). Finally, the initial forward reaction rates when normalized on the number of acid sites per gram ($-r_{0,\,COH/ACID}$) for FeMoP catalysts reduced at 650, 750, and 850 °C were nearly identical at any given reaction temperature (Fig. 2b). Therefore, surface acid sites were the active sites for the dehydration of cyclohexanol.

Kinetic data for the dehydration of cyclohexanol at five temperatures (180, 190, 200, 210, and 220 °C) were evaluated in order to obtain activation energies (E_A) for the FeMoP catalysts. The FeMoP catalysts not only followed Arrhenius behavior under the employed reaction temperatures (Fig. 2b) but all materials also exhibited similar values of E_A (~130 kJ mol^{-1}) in this reaction. Previous studies reported that similar values of E_A suggested a similar pathway for this reaction when using acid catalysts (e.g. HZSM-5 [17], γ-Al_2O_3 [52], and H_3PO_4 [17]). This suggests that all FeMoP materials catalyzed the reaction following a similar mechanistic pathway.

3.2.2. HDO of phenol

The catalytic role of CO-titrated metal sites (N_{CO}) present on the surface of the FeMoP catalysts was investigated using another lignin model compound, phenol ($C_{AROMATIC}$-O, denoted as PHEN), as a probe molecule. These CO-titrated metal sites are likely a combination of near zero-valent metal sites [53,54] and Lewis acid sites (or coordinatively unsaturated sites (CUSs) [30]), both of which could be active sites for the HDO of biomass model compounds [30,55,56]. In this study, phenol dissolved in decane was fed to the reactor packed with the FeMoP catalysts at 400 °C and reacted under a H_2 atmosphere (5.2 MPa). Similar to the dehydration of

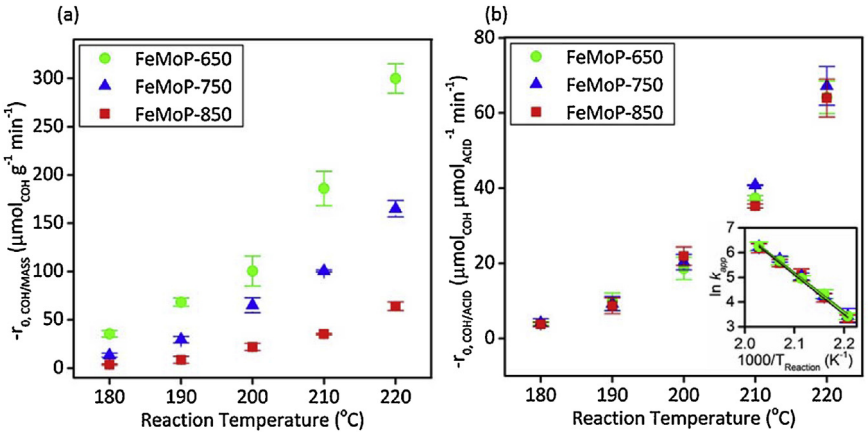

Fig. 2. Initial reaction rate of cyclohexanol dehydration normalized on (a) mass ($-r_{0,COH/MASS}$) (b) and number of acid sites ($-r_{0,COH/ACID}$) at several reaction temperatures. Inset in Fig. 2b shows the fitted Arrhenius plots based on the data plotted in Fig. 2b. The inset in Fig. 2b is a plot of $\ln(k_{app})$ vs $1000/T_{Reaction}$ (K^{-1}).

cyclohexanol, identical amounts (30 mg) of FeMoP catalysts were used in each reaction run to compare the initial reaction rate normalized on the mass of each catalysts ($-r_{0,PHEN/MASS}$) resulting from operation at $X_{PHENOL} \leq \sim 15\%$. Again, to ensure that the reactions were operated in the forward reaction-dominant regime, three control experiments were performed which demonstrated negligible mass and heat transport effects during the reaction runs (Fig. S8). The product selectivity in the forward reaction-dominant regime favored the production of benzene (~90% selectivity) for all FeMoP catalysts at 400 °C (Fig. S9).

Phenol HDO was then performed at varying reaction temperatures, and the results are depicted in Fig. 3. A decrease in $-r_{0,PHEN/MASS}$ was observed on FeMoP catalysts synthesized at higher reduction temperatures (Fig. 3a). Additionally, as noted above (Table 1), the N_{CO} sites decreased on the FeMoP catalysts synthesized at higher reduction temperatures. When these rates were normalized on N_{CO} ($-r_{0,PHEN/CO}$, Fig. 3b), all FeMoP catalysts had similar values of $-r_{0,PHEN/CO}$, which suggested that the CO-titrated metal sites were the primary active sites for the HDO of phenol. The normalization on CO-titrated metal sites was in agreement with previous studies in which surface metals sites (NiMoP [29] and FeNiP [57]) of bimetallic phosphides were suggested as active sites for the HDO of model compounds (e.g. anisole and 2-methyltetrahydrofuran). The $-r_{0,PHEN/CO}$ values for FeMoP-650 were slightly lower than those for FeMoP-750 and FeMoP-850. This could be due to the different accessibility of the reactant to active sites of the much smaller crystallites observed in FeMoP-650 compared to FeMoP-750 and FeMoP-850 (Table 1 and Fig. S4).

Multiple prior studies have investigated two site mechanisms for HDO reactions of various $C_{AROMATIC}$-O model compounds. On Mo_2C surfaces, one distinct metal site has been proposed to coordinate with the aromatic ring in the reactant while another metal site participates in the $C_{AROMATIC}$-O bond cleavage [13,58–60]. Several other studies have proposed that the O functionality in the reactant binds to a hydroxyl or acid site while a reduced metal site facilitates H_2 dissociation used to cleave the $C_{AROMATIC}$-O bond [24,61–63]. Yet another type of mechanism that has been proposed for HDO reactions is a Mars-van Krevelen or reverse Mars-van Krevelen mechanism, which have been reported on oxide catalysts where surface vacancies form to facilitate the reaction [21,64]. For the FeMoP catalysts reported here, it is possible that a surface acid site binds to the —OH in phenol to destabilize the $C_{aromatic}$-O, while reduced metal surface sites dissociate H_2 onto the surface. Using the above kinetic data in conjunction with reported mechanisms in literature [61,63], a two site Langmuir–Hinshelwood mechanism was proposed (Eqs. (4)–(9)), where R, S_1, and S_2 indicate phenyl (C_6H_5) and two surface sites, respectively. H_2 first dissociatively adsorbs on two S_1 sites (Eq. (4)), while phenol adsorbs on S_2 (Eq. (5)). In the following step, a surface bound hydrogen species protonates the absorbed phenol (Eq. (6)), followed by the addition of another surface H species to form benzene (Eq. (7)). Two assumptions were made to link this two-site mechanism to values of $-r_{0,PHEN-MASS}$ on the FeMoP catalysts. Firstly, Eq. (7) was assumed irreversible and the rate-determining step (RDS) [63]. Eq. (6) could also be the RDS, but the derived rate expression in Eq. (10) would have the same form. Secondly, all elementary steps, except Eq. (5), were assumed to be pseudo-steady state, which provided a site-balance involving all chemical species adsorbed on both S_1 and S_2 during the HDO of phenol. The resulting $-r_{PHEN/MASS}$ based on the aforementioned assumptions can be expressed in Eq. (10), where k, K_1, and K_2 denote reaction rate constant, adsorption coefficient for phenol, and adsorption coefficient for H_2, respectively.

$$H_2 + 2S_1 \leftrightarrows 2H - S_1 \quad (4)$$

$$R - OH + S_2 \leftrightarrows R - OH - S_2 \quad (5)$$

$$R - OH - S_2 + H - S_1 \leftrightarrows R - OH_2 - S_2 + S_1 \quad (6)$$

$$R - OH_2 - S_2 \rightarrow OH - S_2 + R - H \quad (7)$$

$$OH - S_2 + H - S_1 \leftrightarrows H_2O - S_2 + S_1 \quad (8)$$

$$H_2O - S_2 \leftrightarrows H_2O + S_2 \quad (9)$$

$$-r_{0,PHEN/MASS} = k\left[\frac{K_1 C_{0,PHEN}}{\left(1 + K_1 C_{0,PHEN}\right)}\right]\left[\frac{\left(K_2 C_{0,H_2}\right)^{\frac{1}{2}}}{\left(1 + \left(K_2 C_{0,H_2}\right)^{\frac{1}{2}}\right)}\right] \quad (10)$$

Eq. (10) could be further simplified based on an additional study where $-r_{0,PHEN/MASS}$ was monitored as a function of $C_{0,H2}$ and $C_{0,PHEN}$ (Fig. 4).

The initial phenol HDO rate ($-r_{0,PHEN/MASS}$) showed 0th-order dependence on the initial hydrogen concentration $C_{0,H2}$ leading to the simplified rate expression in Eq. (11). In this simplification, because the initial hydrogen concentration ($C_{0,H2}$) used during the reaction was far greater than the $C_{0,PHEN}$, the contribution of $C_{0,H2}$ to $-r_{0,PHEN/MASS}$ was assumed constant and therefore incorporated into the value of k' (Eq. (11)).

$$-r_{0,PHEN/MASS} = k'\left[\frac{K_1 C_{0,PHEN}}{\left(1 + K_1 C_{0,PHEN}\right)}\right] \quad (11)$$

Having proposed a mechanism and derived a rate law, data for $-r_{0,PHEN/MASS}$ of FeMoP-650 (Fig. 4) were fitted to a

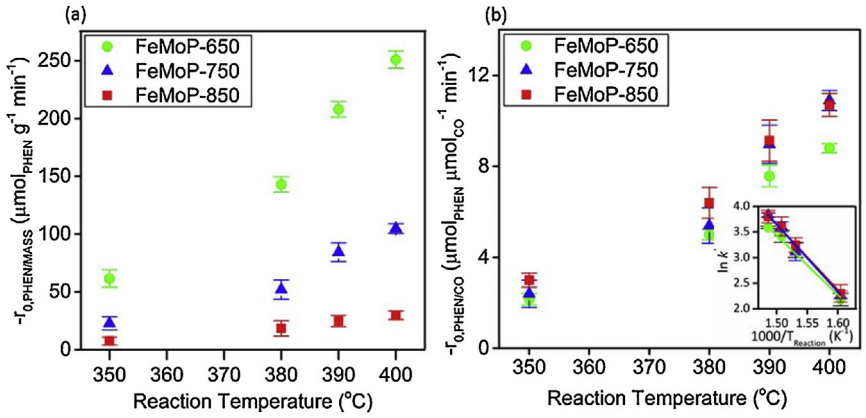

Fig. 3. Initial reaction rates for phenol HDO normalized on (a) mass ($-r_{0,PHEN/MASS}$) and (b) CO-titrated metal sites ($-r_{0,PHEN/CO}$) at various reaction temperatures. Inset in Fig. 3b shows the fitted Arrhenius plots based on the data plotted in Fig. 3b. The inset in Fig. 2b is a plot of $\ln(k')$ vs $1000/T_{Reaction}$ (K^{-1}).

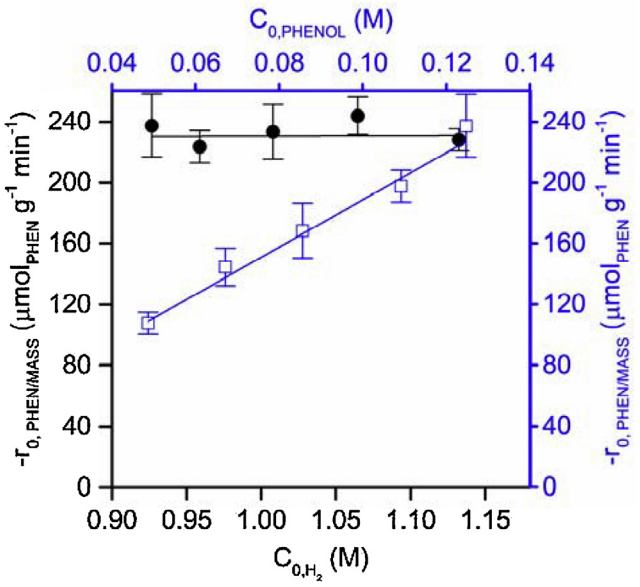

Fig. 4. Plot of $-r_{0,PHEN/MASS}$ at various initial concentrations $C_{0,H2}$ (black circles) and $C_{0,PHEN}$ (blue hollow squares) using FeMoP-650 for the HDO of phenol at 400 °C. (For interpretation of the references to color in this figure legend, the reader is referred to the web version of this article.)

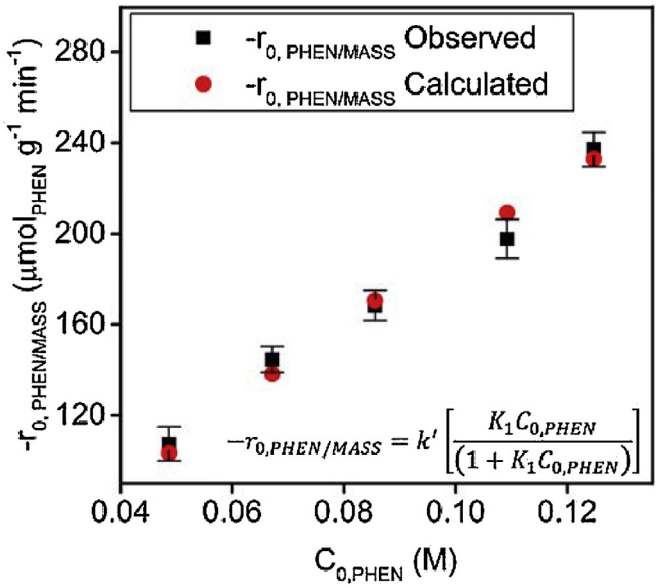

Fig. 5. Initial rate of phenol HDO on FeMoP-650 normalized on mass ($-r_{0,PHEN/MASS}$) fitted to Langmuir-Hinshelwood kinetic model.

Langmuir–Hinshelwood kinetic model with an excellent agreement ($R^2 \sim 0.97$, Fig. 5).

Furthermore, the value of K_1 was extracted from this data, which was determined as 2.0 M^{-1} at 400 °C (Eq. (11)). Considering that the values of $C_{0,PHEN}$ ranged from 0.05 M to 0.13 M, the values of resulting $K_1 C_{0,PHEN}$ were close to unity and could not be neglected. Based on the fitted data in Fig. 5, the value of k' was calculated to be 1160 min^{-1}. Based on the rate expression in Eq. (10), the apparent activation energies (E_A) of the FeMoP catalysts were determined by performing reactions at three additional reaction temperatures (350 °C, 380 °C, and 390 °C). The values of E_A ($\sim$100 kJ mol^{-1}, Fig. 3b) were similar for all FeMoP catalysts, which again implied a similar reaction pathway on these materials. Furthermore, in addition to consistently showing high selectivity to benzene (S_{BEN}) at all reaction temperatures (Fig. S9), the FeMoP catalysts also exhibited values of initial forward rates of phenol normalized on N_{CO} ($-r_{0,PHEN/CO}$) that were almost invariant at each reaction temperature (Fig. 3b). The similar E_A values and $-r_{0,PHEN/CO}$ for all FeMoP catalysts suggested that the FeMoP materials catalyzed the HDO of phenol along a similar reaction pathway [17,52] and, furthermore, the surface metal sites on the FeMoP catalysts were likely the active sites for this reaction.

3.2.3. Mechanistic evaluation

The reaction pathway on the active sites of the FeMoP catalysts (CO-titrated metal sites) was investigated by observing the product selectivities from phenol HDO at different conversions. This was motivated by our previous batch reactions, using anisole as the model $C_{AROMATIC}$-O compound, operated at high values of $X_{ANISOLE}$ (i.e. >25–99%), which showed the FeMoP catalysts synthesized via the reduction at 750 °C or lower led to an increase in aromatic products (e.g. benzene and toluene) compared to the FeMoP analogues synthesized at higher reduction temperatures [27]. As shown in Fig. 6, the FeMoP catalysts showed very different values of S_{BEN} at higher values of X_{PHEN} (e.g., ~70%).

The S_{BEN} on both FeMoP-650 and FeMoP-750 consistently reached values of ~90% throughout the high conversion study. FeMoP-850, in contrast, showed a decrease in values of S_{BEN} from ~90% to ~75%, when increasing the values of X_{PHEN} up to ~70%. The change in product selectivity at different conversions of phenol was likely due to surface coverage of the reactant and product molecules. At lower values of X_{PHEN} the surface is covered primar-

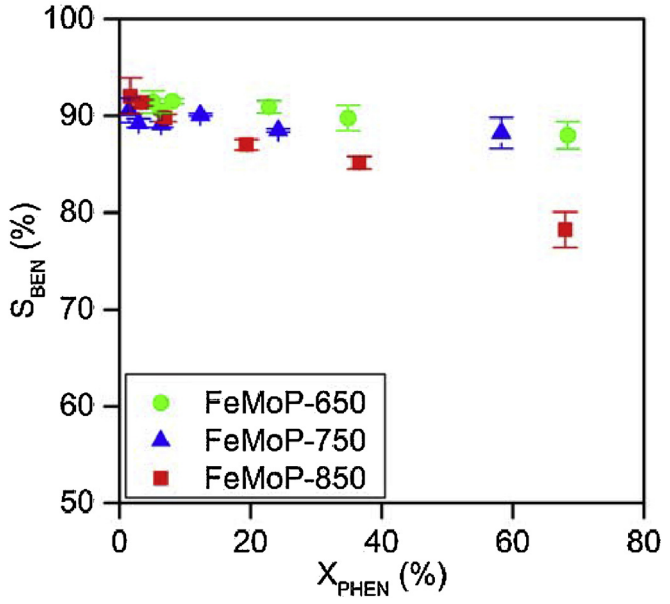

Fig. 6. Selectivity to benzene (S_{BEN}) at various conversions of phenol (X_{PHEN}) on the FeMoP catalysts at 400 °C.

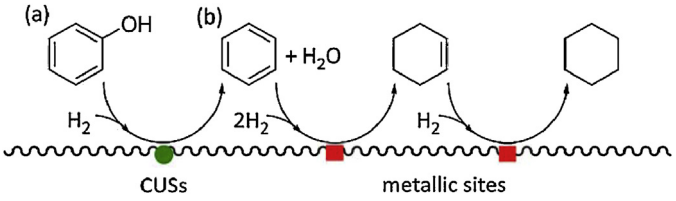

Fig. 7. (a) HDO pathway for CUSs (green circle) and (b) hydrogenation pathway for metallic sites (red square) on the FeMoP surface. (For interpretation of the references to color in this figure legend, the reader is referred to the web version of this article.)

ily with phenol, and thus HDO reactions dominate. At higher values of X_{PHEN}, the increased formation of benzene leads to higher surface coverages of benzene, which would allow for its subsequent hydrogenation on the FeMoP catalysts. One possible reason for the different values of S_{BEN} among the FeMoP catalysts at higher X_{PHEN} are due to the loss of CUSs (i.e. Lewis acid sites) on the FeMoP catalysts synthesized at higher reduction temperatures. Furthermore, the surface characterization in Table 1 shows that FeMoP-650 and FeMoP-750 contained a similar amount of acid and CO-titrated sites, while FeMoP-800 and FeMoP-850 had a higher amount of CO-titrated sites compared to acid sites. Therefore at least two types of metal sites likely existed on the FeMoP catalysts, metallic sites and CUSs (i.e. Lewis acid sites) [30,40]. The CUSs were of particular interest because prior reports with sulfide and phosphide catalysts suggested the CUSs to be the active sites for HDO of model compounds [30,55,56,65]. Additionally, it has been previously proposed in multiple independent studies that metallic sites are capable of hydrogenating aromatic rings to form aliphatic products (i.e. cyclohexane and cyclohexene, denoted as aliphatic) [30,66,67]. Thus it is proposed for these FeMoP materials (and summarized schematically in Fig. 7) that the surface likely contained CUSs that catalyzed the direct HDO of $C_{AROMATIC}$-O, likely leading to the large S_{BEN} for FeMoP-650 [30,55,56], and metallic sites that further hydrogenated the adsorbed $C_{AROMATIC}$, likely resulting in the higher rate of formation of aliphatic products for FeMoP-850 [24,30,50]. Higher reduction temperatures may facilitate the loss of CUSs (i.e. Lewis acid sites) by removing them via heterolytic cleavage of H_2 [44,45], as shown by the decrease in values of N_{ACID} with increasing reduction temperatures (Table 1). Furthermore, previous reports have demonstrated that the key CUSs in molybdenum sulfide catalysts, which are similar in surface properties to phosphide catalysts (i.e. Brønsted, Lewis, and metallic sites), predominantly formed on edges and rims of planes [68–70]. Thus, a reduction of edge and rim atoms compared to surface atoms via sintering could also decrease the number of CUSs relative to metallic surface atoms [68,69]. Therefore, the significant crystallite growth seen in the Scherrer analysis of XRD (Table 1) and morphology change observed in the *in situ* TEM analysis (Fig. S4) could lead to a reduction in the ratio of edge and rim atoms relative to metallic surface atoms, which would ultimately lead to a decrease in aromatic selectivity. Of note, it is possible that the water formed during the HDO of phenol could potentially interact with the surface to influence the acidity and thus the reactivity of the catalysts. This effect was tested by pulsing pure water for intervals of ~15 min during a time-on-stream study while operating at close to 20% phenol conversion using FeMoP-850. From the results shown in Fig. S10, the addition of water did not significantly affect $-r_{0,PHEN/CO}$ or S_{BEN}. Therefore, from these studies, the water produced from the reaction is unlikely to affect the reactivity of the catalysts under these operating conditions.

The HDO and hydrogenation pathways on the FeMoP catalysts were evaluated by co-feeding a reactant mixture of phenol and benzene at 400 °C. For these control experiments, FeMoP-650 and FeMoP-850 were used as the catalysts due to their different S_{BEN} profiles (Fig. 6). In these reactions, phenol (0.13 M) mixed with benzene (30 mol% with respect to the concentration of phenol, or 0.039 M) was used as the feed stream. The 0.039 M concentration of benzene was added in order to mimic the onset of hydrogenated products that were shown in Fig. 6 (S_{BEN} started to decrease at X_{PHEN} of ≥20%). Instead of investigating S_{BEN}, the production rate of cyclohexene and cyclohexane ($r_{ALIPHATIC}$, μmol min^{-1}) was calculated at different residence times (Fig. S11). For the FeMoP-650 and FeMoP-850 catalysts, the addition of benzene to the feed stream decreased X_{PHEN}. It is likely that benzene competitively adsorbed on the surface, which would result in a decreased X_{PHEN}. The addition of benzene to the feed stream also slightly increased the values of $r_{ALIPHATIC}$ for FeMoP-650 (0.12 μmol min^{-1} to 0.34 μmol min^{-1} at ~70% conversion) (Fig. S11). Therefore, benzene could be hydrogenated on the FeMoP-650 catalyst under these conditions. This result also suggested that phenol was first deoxygenated to benzene and then subsequently hydrogenated to aliphatics through tandem reactions. The addition of benzene enhanced the values of $r_{ALIPHATIC}$ for FeMoP-850 (0.76 μmol min^{-1} to 2.54 μmol min^{-1} at ~70% conversion). This large increase in $r_{ALIPHATIC}$ on FeMoP-850 suggested that the decrease in S_{BEN} observed in Fig. 6 was a result of subsequent hydrogenation reactions. Therefore, it is possible that either the hydrogenation sites on FeMoP-850 were more active or present in a higher density (per mass basis) than the hydrogenation sites on FeMoP-650. To verify that FeMoP-850 was more active for benzene hydrogenation than FeMoP-650, reactions were run with only benzene to determine the rate of consumption of benzene ($-r_{0,BEN,CO}$) (Fig. S12). FeMoP-850 was ~2.5 times more active than FeMoP-650 when normalized on CO-titrated sites. The results of these residence time studies were in line with two suggested reaction pathways, shown in Fig. 7, where the acid sites facilitate HDO on phenol followed by benzene hydrogenation on metallic sites (Fig. 8).

3.2.4. Stability in the HDO of phenol

The catalytic stability of FeMoP-650 (catalyst with $-r_{0,PHEN/MASS}$) was examined via a time-on-stream (TOS) study over 48 h under 5.2 MPa of H_2 at 400 °C. For 48 h, FeMoP-650 was able to maintain activity ($-r_{0,PHEN/CO}$ ~9.5 μmol_{PHEN} μmol_{CO}^{-1} min^{-1}) and selectivity (S_{BEN} ~90%), which demonstrated the catalytic stability of FeMoP-650.

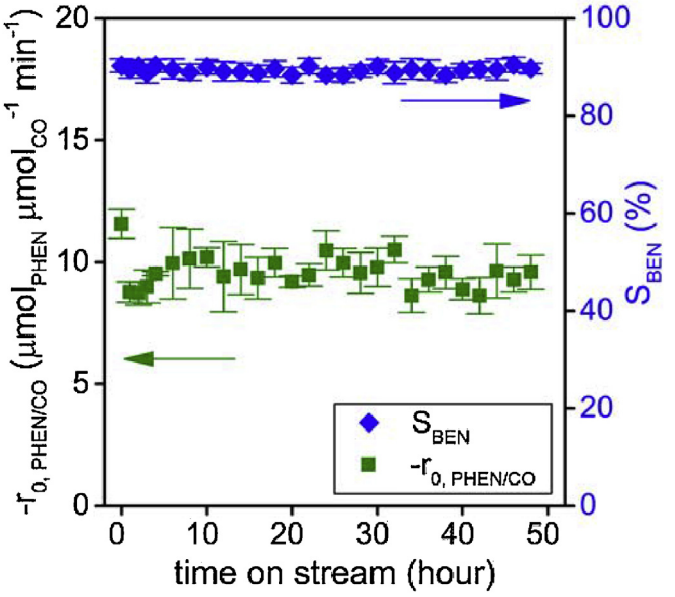

Fig. 8. TOS study of the FeMoP-650 catalyst for the HDO of phenol.

The catalytic stability of FeMoP-650 after the TOS run was further investigated using XPS in order to study the change in oxidation state of the surface species. The resulting XP spectrum was compared with that prior to the TOS run in order to determine if the surface of FeMoP-650 was altered due to the reaction conditions (Fig. S13). The C 1 s region in the XP spectrum after the TOS run was first observed to investigate the potential formation of surface carbidic species that have been reported as active species for this reaction [71–73]. The XP spectrum did not show a peak associated with surface carbidic species (located at binding energies between 280 and 283 eV). Therefore, the possible role of surface carbidic species to catalyze this reaction was excluded. In addition, the other surface elements observed in the regions of Fe 2p $_{3/2}$, Mo 3d $_{5/2}$, and P 2p $_{3/2}$, were composed of two surface species (i.e. near zero-valent species and oxidized species [53]). For the reduced surface species, their oxidation states were retained throughout the TOS run, as evidenced by unchanged binding energies in the XP spectra ($Fe^{\delta+}$ at ~706.7 eV; $Mo^{\delta+}$ at ~227.6 eV; $P^{\delta-}$ at ~129.2 eV) [53,54,74]. In contrast, oxidized surface species were reduced during the TOS run, as demonstrated by the decrease in binding energies of these oxidized species. During the TOS run, surface P species assigned to phosphate (at 133.5 eV) were also reduced to generate surface species assigned to pyrophosphate species (132.7 eV) [27]. In particular, surface species of Fe^{3+} (at 711.1 eV) and Mo^{6+} (at 232.1 eV) inherent to the FeMoP-650 were reduced to Fe^{2+} (710.2 eV) and Mo^{5+} (230.7 eV). These results suggested that the oxidized surface species underwent an *in situ* reduction during the reaction due to the presence of elevated pressure H_2. Therefore FeMoP-650 showcased enhanced catalytic stability due to *in situ* reduction of the surface, which prevented complete surface oxidation and deactivation.

4. Conclusions

In summary, we have studied the multifunctional surface characteristics of FeMoP catalysts as they pertain to the deoxygenation of biomass model compounds. The surface properties were altered by changing the reduction temperature used during the catalyst syntheses (650–850 °C). It was determined that the materials with the highest acidity (ρ_{ACID}) and CO-titrated metal sites (N_{CO}) were attainable at the lowest reduction temperatures. These FeMoP materials acted as non-aqueous phase acid catalysts for the dehydration of cyclohexanol at 180 and 220 °C, and FeMoP-650 showed the highest mass normalized rate due to the largest amount of surface acid species. All FeMoP catalysts yielded similar activation energy values for the dehydration of cyclohexanol (~130 kJ mol^{-1}), which suggested that all FeMoP catalysts followed a similar reaction pathway. In addition, the CO-titrated surface metal sites were studied via hydrodeoxygenation (HDO) of phenol at 350–400 °C. At conversions <15%, all FeMoP catalysts were ~90% selective to benzene and displayed similar activation energies (~100 kJ mol^{-1}), suggesting a similar HDO reaction pathway on these FeMoP catalysts. However, at conversions >20% the selectivity to benzene decreased on FeMoP-850. When benzene was added into the feed stream, FeMoP-650 favored HDO of phenol with minimal hydrogenation of benzene while FeMoP-850 was significantly more active for the hydrogenation of benzene to aliphatic compounds. The high selectivity to benzene on FeMoP-650 was potentially due to the increased number of coordinatively unsaturated sites, which could be altered based on reduction temperature. Furthermore, the FeMoP catalysts provided long-term stability due in part to *in situ* reduction of surface species in the presence of H_2 gas, as evidenced by a 48 h time-on-stream study and XP spectra after the reaction. Therefore, based on the high selectivities to the aromatic product and high catalytic stability, FeMoP is highly applicable to other lignocellulosic biomass relevant deoxygenation reactions.

Acknowledgements

We thank NSF for support through the CAREER program (CBET-1351609). We also thank the ND Energy Materials Characterization Facility for the use of the XRD and XPS, the Center for Environmental Science and Technology (CEST) at the University of Notre Dame, and Notre Dame Integrated Imaging Facilities (NDIIF) for partial support in utilizing their instrumentation. We thank Dr. Rouvimov and DENSsolutions for their time and expertise in acquiring the images from the *in situ* TEM work. We also thank Dr. Paul McGinn for valuable conversations and use of his crystallographic software. We acknowledge VESTA 3 and Mercury CSD for access to their three-dimensional visualization of crystal, volumetric, and morphology data.

Appendix A. Supplementary data

Supplementary data associated with this article can be found, in the online version, at http://dx.doi.org/10.1016/j.apcata.2016.06.011.

References

[1] D.M. Alonso, S.G. Wettstein, J.A. Dumesic, Chem. Soc. Rev. 41 (2012) 8075–8098.
[2] E. Furimsky, Catal. Today (2013).
[3] J.C. Hicks, J. Phys. Chem. Lett. 2 (2011) 2280–2287.
[4] H. Li, S. Pattathil, M.B. Foston, S.-Y. Ding, R. Kumar, X. Gao, A. Mittal, J.M. Yarbrough, M.E. Himmel, A.J. Ragauskas, M.G. Hahn, C.E. Wyman, Biotechnol. Biofuels 7 (2014) 1–11.
[5] K. Barta, P.C. Ford, Acc. Chem. Res. 47 (2014) 1503–1512.
[6] P.C.A. Bruijnincx, B.M. Weckhuysen, Nat. Chem. 6 (2014) 1035–1036.
[7] Y. Romero, F. Richard, S. Brunet, Appl. Catal. B Environ. 98 (2010) 213–223.
[8] V.N. Bui, D. Laurenti, P. Afanasiev, C. Geantet, Appl. Catal. B Environ. 101 (2011) 239–245.
[9] C. Zhao, Y. Kou, A.A. Lemonidou, X. Li, J.A. Lercher, Angew. Chem. Int. Ed. 48 (2009) 3987–3990.
[10] N. Yan, Y. Yuan, R. Dykeman, Y. Kou, P.J. Dyson, Angew. Chem. Int. Ed. 49 (2010) 5549–5553.
[11] W. Zhang, J. Chen, R. Liu, S. Wang, L. Chen, K. Li, ACS Sustainable Chem. Eng. 2 (2014) 683–691.
[12] T. Omotoso, S. Boonyasuwat, S.P. Crossley, Green Chem. 16 (2014) 645–652.
[13] W.-S. Lee, Z. Wang, R.J. Wu, A. Bhan, J. Catal. 319 (2014) 44–53.
[14] J. Kim, G.T. Neumann, N.D. McNamara, J.C. Hicks, J. Mater. Chem. A 2 (2014) 14014–14027.

[15] H. Wang, J. Male, Y. Wang, ACS Catal. 3 (2013) 1047–1070.
[16] C. Zhao, W. Song, J.A. Lercher, ACS Catal. 2 (2012) 2714–2723.
[17] J. He, C. Zhao, J.A. Lercher, J. Catal. 309 (2014) 362–375.
[18] C. Zhao, S. Kasakov, J. He, J.A. Lercher, J. Catal. 296 (2012) 12–23.
[19] M. Badawi, J.F. Paul, S. Cristol, E. Payen, Y. Romero, F. Richard, S. Brunet, D. Lambert, X. Portier, A. Popov, E. Kondratieva, J.M. Goupil, J. El Fallah, J.P. Gilson, L. Mariey, A. Travert, F. Maugé, J. Catal. 282 (2011) 155–164.
[20] B.M. Vogelaar, N. Kagami, T.F. van der Zijden, A.D. van Langeveld, S. Eijsbouts, J.A. Moulijn, J. Mol. Cat. A Chem. 309 (2009) 79–88.
[21] T. Prasomsri, T. Nimmanwudipong, Y. Roman-Leshkov, Energy Environ. Sci. 6 (2013) 1732–1738.
[22] P.M. Mortensen, H.W.P. de Carvalho, J.-D. Grunwaldt, P.A. Jensen, A.D. Jensen, J. Catal. 328 (2015) 208–215.
[23] R. Rousseau, D.A. Dixon, B.D. Kay, Z. Dohnalek, Chem. Soc. Rev. 43 (2014) 7664–7680.
[24] X. Zhu, L.L. Lobban, R.G. Mallinson, D.E. Resasco, J. Catal. 281 (2011) 21–29.
[25] S.T. Oyama, T. Gott, H. Zhao, Y.-K. Lee, Catal. Today 143 (2009) 94–107.
[26] R. Prins, M. Bussell, Catal. Lett. (2013) 1–24.
[27] D.J. Rensel, S. Rouvimov, M.E. Gin, J.C. Hicks, J. Catal. 305 (2013) 256–263.
[28] H.Y. Zhao, D. Li, P. Bui, S.T. Oyama, Appl. Catal. A 391 (2011) 305–310.
[29] K. Li, R. Wang, J. Chen, Energy Fuels 25 (2011) 854–863.
[30] V.M.L. Whiffen, K.J. Smith, Energy Fuels 24 (2010) 4728–4737.
[31] Y. Yang, A. Gilbert, C. Xu, Appl. Catal. A 360 (2009) 242–249.
[32] S. Ted Oyama, H. Zhao, H.J. Freund, K. Asakura, R. Włodarczyk, M. Sierka, J. Catal. 285 (2012) 1–5.
[33] R. Wang, K. Smith, Catal. Lett. 144 (2014) 1594–1601.
[34] P. Bui, J.A. Cecilia, S.T. Oyama, A. Takagaki, A. Infantes-Molina, H. Zhao, D. Li, E. Rodríguez-Castellón, A. Jiménez López, J. Catal. 294 (2012) 184–198.
[35] A.P. Grosvenor, R.G. Cavell, A. Mar, J. Solid State Chem. 181 (2008) 2549–2558.
[36] S. Diplas, O.M. Løvvik, J. Phys. Condens. Matter. 21 (2009) 245503.
[37] B.J. Tan, K.J. Klabunde, P.M.A. Sherwood, Chem. Mater. 2 (1990) 186–191.
[38] M. Shetty, K. Murugappan, T. Prasomsri, W.H. Green, Y. Román-Leshkov, J. Catal. 331 (2015) 86–97.
[39] X. Wang, P. Clark, S.T. Oyama, J. Catal. 208 (2002) 321–331.
[40] Y.-K. Lee, S.T. Oyama, J. Catal. 239 (2006) 376–389.
[41] F. Al-Kharafi, H. Al-Kandari, A. Katrib, Catal. Lett. 123 (2008) 269–275.
[42] B. Hou, H. Zhang, H. Li, Q. Zhu, Chin. J. Chem. Eng. 20 (2012) 10–17.
[43] E. Muneyama, A. Kunishige, K. Ohdan, M. Ai, J. Catal. 158 (1996) 378–384.
[44] P. Hirunsit, K.-i. Shimizu, R. Fukuda, S. Namuangruk, Y. Morikawa, M. Ehara, J. Phys. Chem. C 118 (2014) 7996–8006.
[45] S. Klacar, H. Gronbeck, Catal. Sci. Technol. 3 (2013) 183–190.
[46] A. Seidel, A. Gutsze, B. Boddenberg, Chem. Phys. Lett. 275 (1997) 113–118.
[47] V.A. Nasluzov, V.V. Rivanenkov, A.M. Shor, K.M. Neyman, U. Birkenheuer, N. Rösch, Int. J. Quantum Chem. 90 (2002) 386–402.
[48] B. Katryniok, S. Paul, F. Dumeignil, ACS Catal. 3 (2013) 1819–1834.
[49] S. Sato, F. Sato, H. Gotoh, Y. Yamada, ACS Catal. 3 (2013) 721–734.
[50] C. Zhao, J. He, A.A. Lemonidou, X. Li, J.A. Lercher, J. Catal. 280 (2011) 8–16.
[51] A. Vjunov, M.Y. Hu, J. Feng, D.M. Camaioni, D. Mei, J.Z. Hu, C. Zhao, J.A. Lercher, Angew. Chem. Int. Ed. 53 (2014) 479–482.
[52] H. Knözinger, H. Bühl, K. Kochloefl, J. Catal. 24 (1972) 57–68.
[53] A.P. Grosvenor, S.D. Wik, R.G. Cavell, A. Mar, Inorg. Chem. 44 (2005) 8988–8998.
[54] A.P. Grosvenor, R.G. Cavell, A. Mar, J. Solid State Chem. 180 (2007) 2702–2712.
[55] M. Badawi, J.-F. Paul, E. Payen, Y. Romero, F. Richard, S. Brunet, A. Popov, E. Kondratieva, J.-P. Gilson, L. Mariey, A. Travert, F. Maugé, Oil Gas Sci. Technol. 68 (2013) 829–840.
[56] A.Y. Bunch, X. Wang, U.S. Ozkan, Appl. Catal. A 346 (2008) 96–103.
[57] A. Cho, J. Shin, A. Takagaki, R. Kikuchi, S. Oyama, Top Catal. 55 (2012) 969–980.
[58] X. Liu, A. Tkalych, B. Zhou, A.M. Köster, D.R. Salahub, J. Phys. Chem. C 117 (2013) 7069–7080.
[59] A.S. Rocha, A.B. Rocha, V.T. da Silva, Appl. Catal. A 379 (2010) 54–60.
[60] B. Zhou, X. Liu, J. Cuervo, D.R. Salahub, Struct. Chem. 23 (2012) 1459–1466.
[61] X. Zhu, L. Nie, L.L. Lobban, R.G. Mallinson, D.E. Resasco, Energy Fuels 28 (2014) 4104–4111.
[62] Y. Hong, H. Zhang, J. Sun, K.M. Ayman, A.J.R. Hensley, M. Gu, M.H. Engelhard, J.-S. McEwen, Y. Wang, ACS Catal. 4 (2014) 3335–3345.
[63] R.C. Nelson, B. Baek, P. Ruiz, B. Goundie, A. Brooks, M.C. Wheeler, B.G. Frederick, L.C. Grabow, R.N. Austin, ACS Catal. 5 (2015) 6509–6523.
[64] D.R. Moberg, T.J. Thibodeau, F.G. Amar, B.G. Frederick, J. Phys. Chem. C 114 (2010) 13782–13795.
[65] A.Y. Bunch, U.S. Ozkan, J. Catal. 206 (2002) 177–187.
[66] J.A. Widegren, M.A. Bennett, R.G. Finke, J. Am. Chem. Soc. 125 (2003) 10301–10310.
[67] A.C.A. Monteiro-Gezork, R. Natividad, J.M. Winterbottom, Catal. Today 130 (2008) 471–485.
[68] M. Daage, R.R. Chianelli, J. Catal. 149 (1994) 414–427.
[69] S. Kasztelan, H. Toulhoat, J. Grimblot, J.P. Bonnelle, Appl. Catal. 13 (1984) 127–159.
[70] E.J.M. Hensen, P.J. Kooyman, Y. van der Meer, A.M. van der Kraan, V.H.J. de Beer, J.A.R. van Veen, R.A. van Santen, J. Catal. 199 (2001) 224–235.
[71] I.N. Shabanova, V.A. Trapeznikov, J. Electron. Spectros. Relat. Phenom. 6 (1975) 297–307.
[72] L. Ramqvist, K. Hamrin, G. Johansson, A. Fahlman, C. Nordling, J. Phys. Chem. Solids 30 (1969) 1835–1847.
[73] C.S. Kuivila, J.B. Butt, P.C. Stair, Appl. Surf. Sci. 32 (1988) 99–121.
[74] P.E.R. Blanchard, A.P. Grosvenor, R.G. Cavell, A. Mar, J. Mater. Chem. 19 (2009) 6015–6022.